Velocity-independent time-domain seismic imaging using local event slopes[a]

[a]Published in Geophysics, 72, no. 3, S139-S147, (2007)

Sergey Fomel

ABSTRACT

I show that, by estimating local event slopes in prestack seismic reflection data, it is possible to accomplish all common time-domain imaging tasks, from normal moveout to prestack time migration, without the need to estimate seismic velocities or any other attributes. Local slopes contain complete information about the reflection geometry. Once they are estimated, seismic velocities and all other moveout parameters turn into data attributes and are directly mappable from the prestack data domain into the time-migrated image domain. I develop an analytical theory for this method and demonstrate its applicability on synthetic and field data examples.

INTRODUCTION

The conventional approach to seismic data analysis (Yilmaz, 2000) consists of two main steps: estimating seismic velocities (the subsurface macromodel) and seismic imaging (mapping of the reflected seismic energy to the reflector positions). The two steps can be repeated when the velocity model gets refined by imaging. Estimating velocities remains one of the most labor-intensive and time-consuming tasks in seismic data processing although several approaches have been developed to partially automate and simplify it (Adler and Brandwood, 1999; Siliqi et al., 2003; Lambaré et al., 2004b). In time-domain imaging, effective seismic velocities are picked from semblance scans. More than just a single parameter (such as seismic velocity) needs to be picked to use higher-order traveltime approximations such as those suggested by the multifocusing approach (Landa et al., 1999; Hertweck et al., 2004).

The idea of *velocity-independent time-domain seismic imaging* belongs to Ottolini (1983), who considered decomposing seismic data into a range of local slopes. Wolf et al. (2004) observed that it is possible to perform moveout analysis by estimating local data slopes in the prestack data domain using an automatic method such as plane-wave destruction (Fomel, 2002). In this paper, I extend Ottolini's idea of velocity-independent imaging and show that extracting local event slopes in prestack data is sufficient for accomplishing all common time-domain imaging tasks, from hyperbolic and non-hyperbolic normal moveout corrections to dip moveout and prestack

time migration. Rather than being a prerequisite for seismic imaging, seismic velocities turn into data attributes that can be extracted from the input data simultaneously with imaging.

The idea of using local event slopes estimated from prestack seismic data goes back to the work of Rieber (1936) and Riabinkin (1957). It was used later by Sword (1987b) and extended in the method of stereotomography (Billette and Lambaré, 1998; Billette et al., 2003; Lambaré et al., 2004a; Lambaré, 2004). In the depth imaging context, local data slopes were also utilized by Baina et al. (2003) for anti-aliased Kirchhoff migration and by Hua and McMechan (2003) in the method of parsimonious depth migration. In this paper, I extend and formalize the application of these ideas to time-domain imaging. By analogy with the oriented wave equation, which describes wave propagation in the space of local orientations (Fomel, 2003a), I use the term *oriented* when referring to local slopes.

The analysis proceeds from normal moveout (NMO) to dip moveout (DMO) and prestack time migration. I derive analytical expressions for mapping the data attributes to the imaging domain and demonstrate their use with synthetic and field data tests.

ORIENTED TIME-DOMAIN IMAGING

Let us start with a simple hyperbolic moveout correction and then consider a progression of time-domain imaging operators with increasing complexity.

Normal moveout

Let us consider the classic hyperbolic model of reflection moveout:

$$t(l) = \sqrt{t_0^2 + \frac{l^2}{v_n^2(t_0)}} \; , \tag{1}$$

where t_0 is the zero-offset traveltime, $t(l)$ is the corresponding traveltime recorded at offset l, and $v_n(t_0)$ is the stacking or RMS velocity. As follows from equation 1, the traveltime slope $p = dt/dl$ is given by

$$p = \frac{l}{t\, v_n^2(t_0)} \; . \tag{2}$$

Knowing the local slope $p(t,l)$ in a common-midpoint gather, one can effectively eliminate the velocity $v(t_0)$ from equations 1 and 2 arriving at the velocity-independent moveout equation (Ottolini, 1983)

$$t_0 = \sqrt{t^2 - t\, p(t,l)\, l} \; . \tag{3}$$

Equation 3 describes a direct mapping from prestack data to the zero-offset time. This equation constitutes an *oriented normal moveout* correction. As follows from equation 2, the velocity is mapped as follows:

$$\frac{1}{v_n^2} = p(t,l)\,\frac{t}{l}\ . \tag{4}$$

Unlike its role in the conventional normal moveout (NMO), velocity is not a requirement for the moveout correction but rather a data attribute derived from the local slopes and mappable directly to the appropriate zero-offset time.

A simple synthetic example is shown in Figure 1. The synthetic data (Figure 1a) were generated by applying inverse NMO with time-variable velocity and represent perfectly hyperbolic events. Figure 1b shows local event slopes measured from the data using the plane-wave destruction algorithm of Fomel (2002). Plane-wave destruction (Claerbout, 1992) works by making a prediction of each seismic trace from the neighboring trace along local slopes and then minimizing the prediction error by an iterative regularized least-squares optimization. Regularization controls smoothness of the estimated slope field. In this work, I use shaping regularization (Fomel, 2007) for an optimal smoothness control. Figure 1c shows the output of oriented NMO using equation 3. As expected, all events are perfectly flattened after NMO.

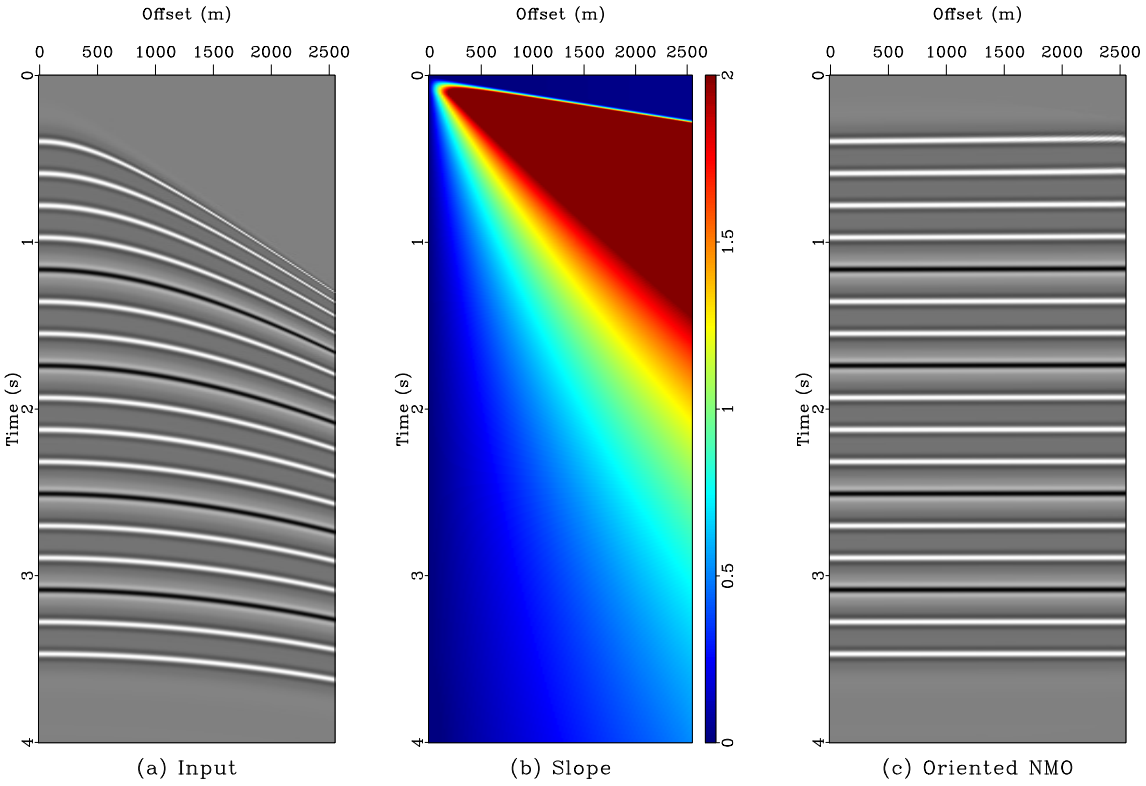

Figure 1: a: A synthetic CMP gather composed of hyperbolas. b: Estimated local event slopes. c: The output of oriented velocity-independent NMO.

In conventional NMO processing, one scans a number of velocities, performs the corresponding number of moveout corrections, and picks the velocity trend from velocity spectra. In oriented processing, velocity becomes, according to equation 4, a data attribute rather than a prerequisite for imaging. Figure 2 shows a comparison between velocity spectra used for picking velocities in the conventional NMO processing and the velocity attribute mapped directly from the data space using equations 3 and 4. A noticeably higher resolution of the oriented map follows from the fact that only the true signal slopes are identified by the slope estimation algorithm. The slope uncertainty, unlike the velocity uncertainty, is not taken into account.

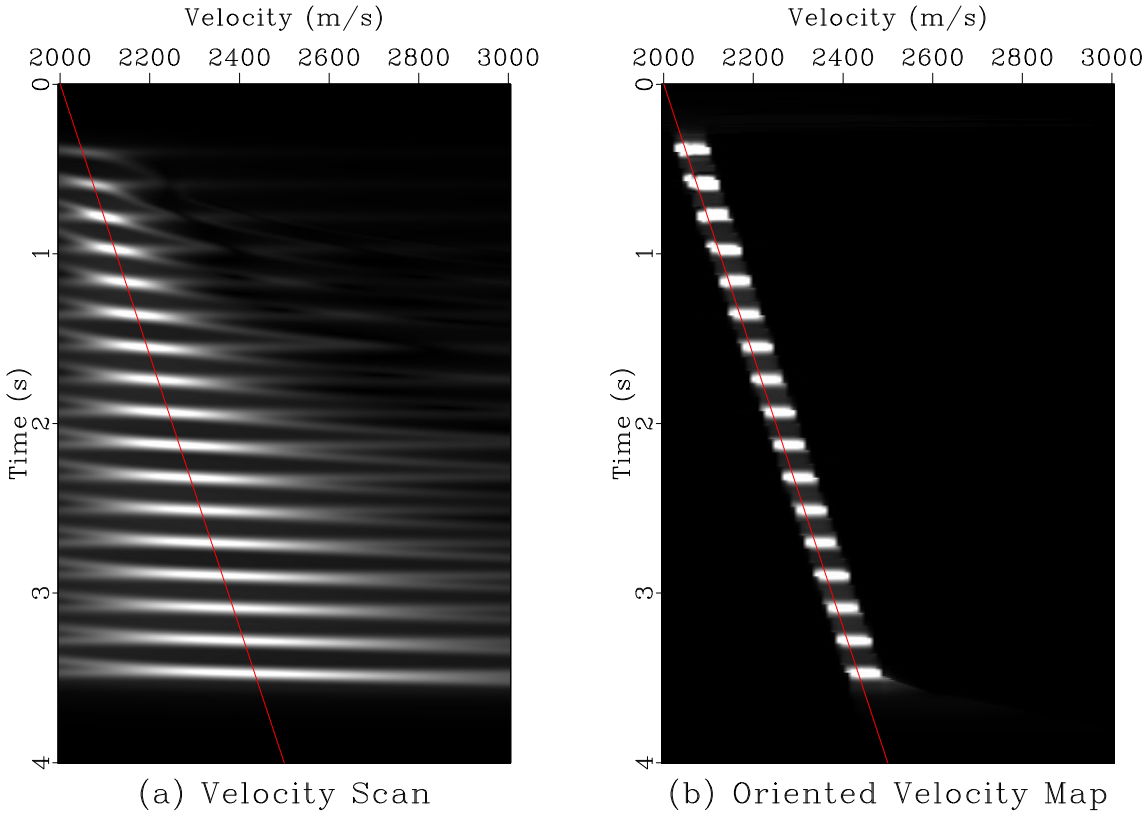

Figure 2: a: Velocity spectra using conventional velocity scanning. In the conventional NMO processing, the velocity trend is picked from velocity spectra prior to NMO. b: Velocity mapped from the data space using oriented NMO. The input for both plots is the synthetic CMP gather shown in Figure 1a. The red line indicates the exact velocity used for generating the synthetic data.

Figure 3 shows a field data example. The data are taken from a historic Gulf of Mexico dataset (Claerbout, 2005). Analogously to the synthetic case, a CMP gather (Figure 3a) is properly flattened (Figure 3c) by an application of oriented NMO using the local event slopes (Figure 3b) measured directly from the data. A comparison between conventional velocity spectra and the velocity mapping with oriented NMO is shown in Figure 4. Again, a significantly higher resolution is observed.

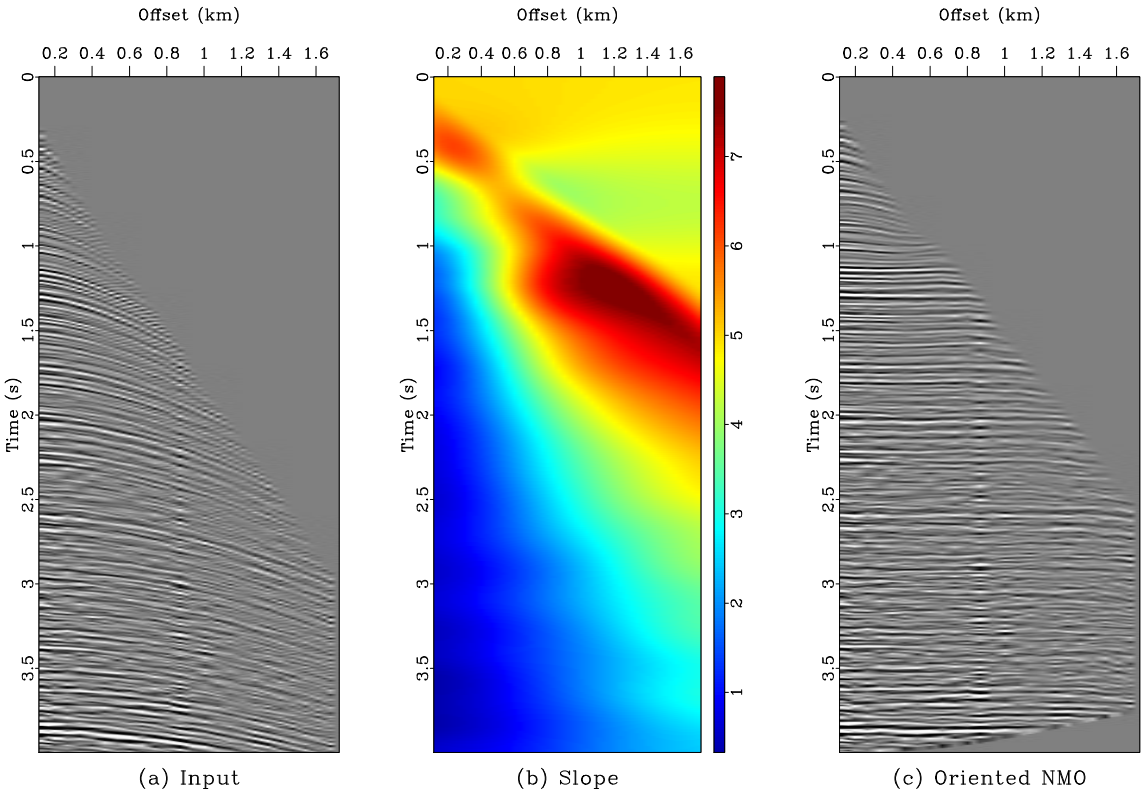

Figure 3: a: A CMP gather from the Gulf of Mexico. b: estimated local event slopes. c: the output of oriented velocity-independent NMO.

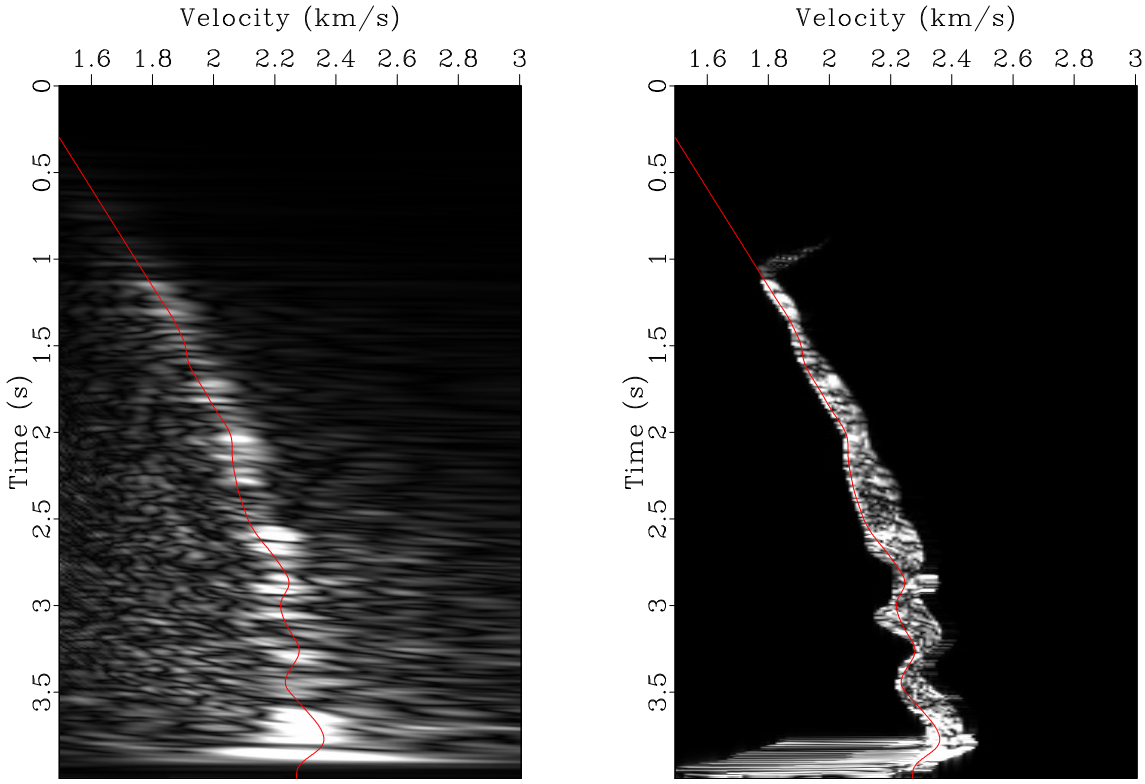

(a) Velocity Scan (b) Oriented Velocity Map

Figure 4: a: Velocity spectra using conventional velocity scanning. In the conventional NMO processing, the velocity trend is picked from velocity spectra prior to NMO. b: Velocity mapped from the data space using oriented NMO. The input for both plots is the CMP gather shown in Figure 3a. The red curve is an automatic pick of the velocity trend shown for comparison.

τ-p NMO

One can choose to perform normal moveout in the slant-stack (τ-p) domain rather than the original t-x domain. In the τ-p domain, hyperbolas turn into ellipses but the moveout correction problem remains (Stoffa et al., 1981). Differentiating the τ-p moveout equation

$$\tau(p) = \tau_0 \sqrt{1 - p^2\, v_n^2(\tau_0)} \tag{5}$$

leads to

$$r = \frac{d\tau}{dp} = -\frac{p\, v_n^2(\tau_0)\, \tau_0^2}{\tau}\ , \tag{6}$$

which resolves in the oriented velocity-free moveout equation analogous to equation 3

$$\tau_0 = \sqrt{\tau^2 - \tau\, r(\tau, p)\, p}\ . \tag{7}$$

Combining equations 5 and 7 produces the corresponding velocity mapping equation

$$v_n^2 = \frac{r(\tau, p)}{p^2\, r(\tau, p) - p\, \tau}\ . \tag{8}$$

Non-hyperbolic moveout

The hyperbolic model 1 is not accurate at large offsets in the case of non-hyperbolic moveouts, caused by vertical or lateral heterogeneity, reflector curvature, or anisotropy (Fomel and Grechka, 2001). One popular model for describing non-hyperbolic moveouts was developed by Malovichko (1978) and has the form of a shifted hyperbola (de Bazelaire, 1988; Castle, 1994; Siliqi and Bousquié, 2000)

$$t(l) = t_0 \left(1 - \frac{1}{S(t_0)}\right) + \frac{1}{S(t_0)} \sqrt{t_0^2 + S(t_0)\, \frac{l^2}{v_n^2(t_0)}}\ , \tag{9}$$

Equation 9 contains an additional parameter S, which is related to heterogeneity and anisotropy of seismic velocities. We can eliminate this parameter by differentiating the equation twice and defining the second derivative $q = \partial p/\partial l = \partial^2 t/\partial l^2$. Eliminating both v_n and S from equation 9 and equations

$$p = \frac{l}{[t_0 + S(t_0)\ (t - t_0)]\ v_n^2}\ , \tag{10}$$

$$q = \frac{t_0^2}{[t_0 + S(t_0)\ (t - t_0)]^3\ v_n^2} \tag{11}$$

leads to the velocity-independent non-hyperbolic moveout equation

$$t_0 = t - \frac{p\, l}{1 + \sqrt{\frac{q\, l}{p}}}\ . \tag{12}$$

If moveout parameters v_n and S are required for subsequent interpretation, one can easily extract them as special data attributes

$$\frac{1}{v_n^2} = t_0 \sqrt{\frac{p^3}{q\,l^3}}\,, \tag{13}$$

$$S = 1 + \frac{p\,(t - p\,l) - q\,l\,t}{\sqrt{q\,p^3\,l^3}}\,. \tag{14}$$

One could estimate the function $q(t,l)$ in practice by numerically differentiating the local slope field $p(t,l)$.

Dix inversion

Not only moveout velocities but also interval velocities can be estimated by using the local slope information. Employing the Dix inversion approach (Dix, 1955) and defining $p_t = \partial p/\partial t$, one can deduce from equations 3 and 4 an expression for the interval velocity v_i, which becomes another attribute directly mappable from the data, as follows:

$$v_i^2 = \frac{l}{p^2\,t}\,\frac{p\,l(p + t\,p_t) - 2p_t\,t^2}{2\,t - l\,(p + t\,p_t)}\,. \tag{15}$$

Equation 15 shows that then the interval velocity can be regarded as another attribute mappable directly from the data. The derivation is detailed in Appendix A.

Figure 5 shows the interval velocity mapping according to equation 15 for the synthetic data example shown in Figure 1a. The exact interval velocity profile (red curve) is recovered perfectly. An analogous example for the field dataset from Figure 3 is shown in Figure 6. The field data result is noisy because of the instability of numerical differentiation but clearly shows the overall range of interval velocities.

Equation 15 enables direct mapping from data slope attributes into interval velocities. Thus, it provides an analytical solution to the stereotomography problem (Billette and Lambaré, 1998) for the special case of horizontal reflection layers and vertically variable velocities.

Migration to zero offset

NMO correction accomplishes mapping to zero offset in the case of horizontal reflectors. Taking account of the reflector dip effect requires dip moveout (Hale, 1995). Combined with NMO, dip moveout maps the input data in time-offset-midpoint coordinates $\{t, h, y\}$ to time-midpoint coordinates $\{t_0, y_0\}$ at the zero-offset section. The corresponding oriented mapping, derived in Appendix B, is

$$t_0^2 = t\,\frac{\left[(t - h\,p_h)^2 - h^2\,p_y^2\right]^2}{(t - h\,p_h)^3}\,, \tag{16}$$

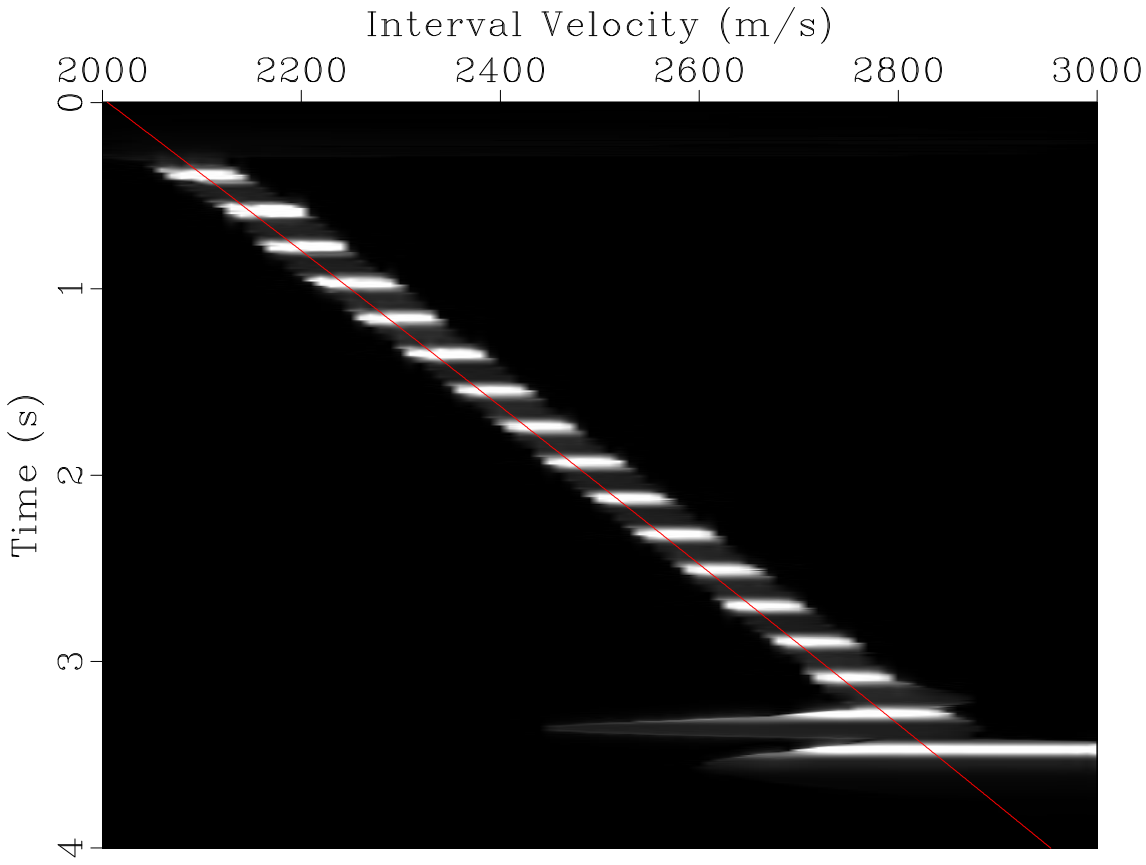

Figure 5: Oriented mapping to interval velocity for the synthetic data set shown in Figure 1a. The exact interval velocity profile is shown by a red curve.

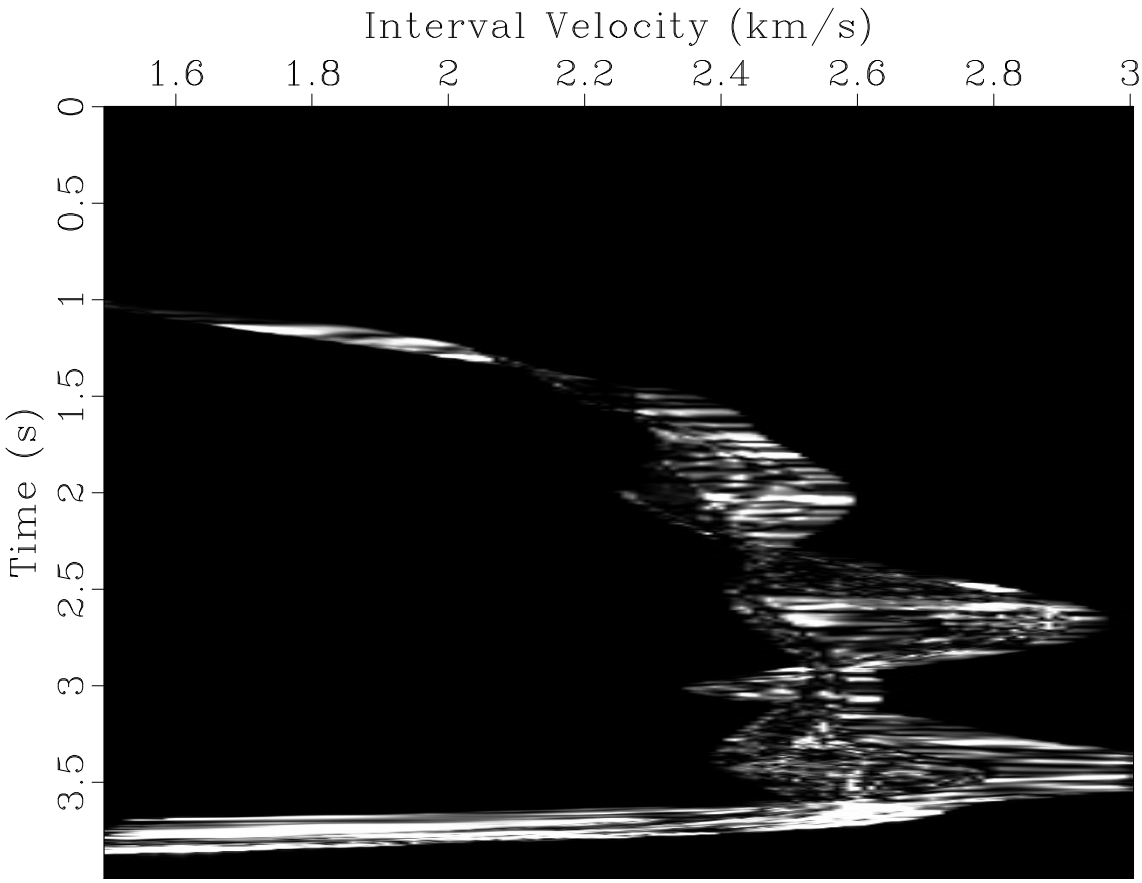

Figure 6: Oriented mapping to interval velocity for the field data set shown in Figure 3a.

$$y_0 \quad = \quad y - \frac{h^2\, p_y}{t - h\, p_h} \;, \tag{17}$$

where $h = l/2$, and $p_h = \partial t/\partial h$ and $p_y = \partial t/\partial y$ are prestack slopes.

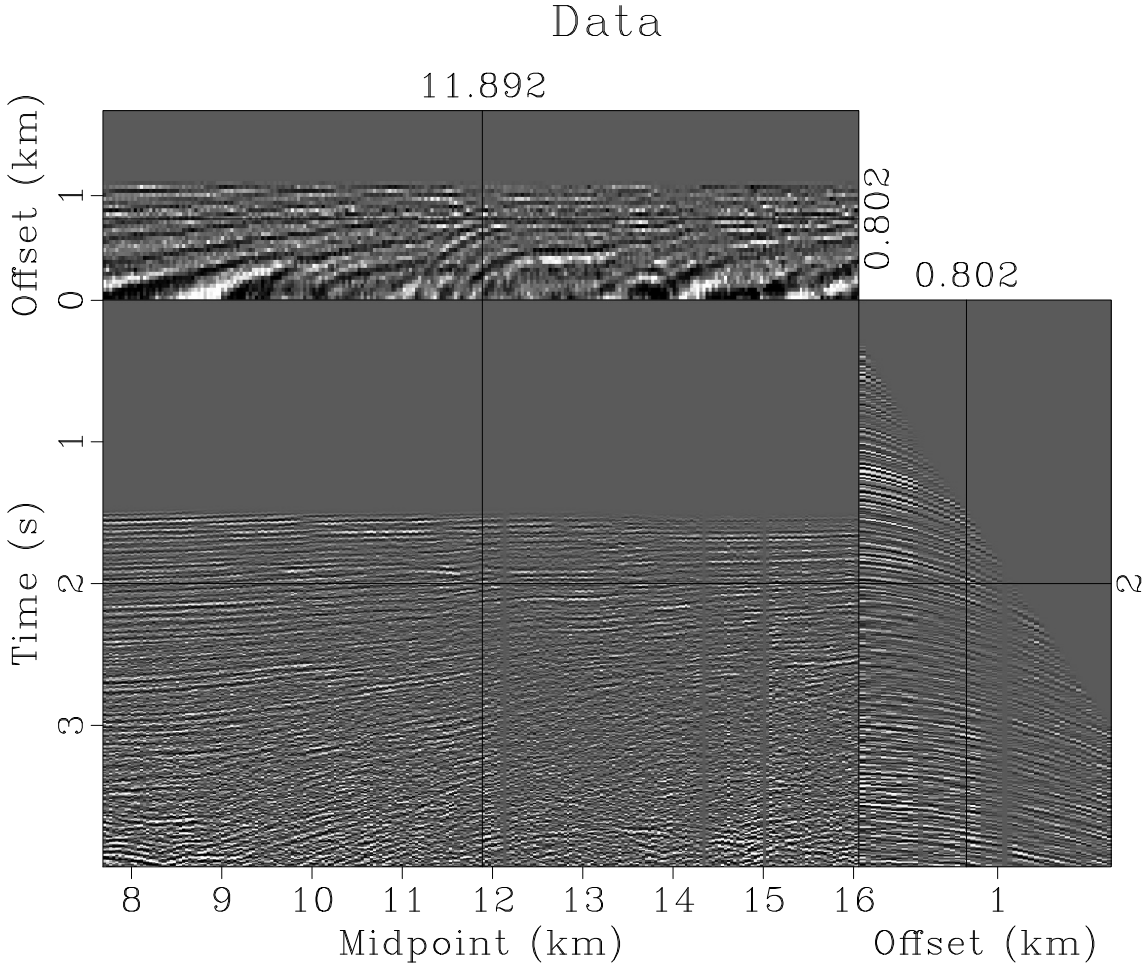

Figure 7: A field 2-D dataset from the Gulf of Mexico used for numerical experiments. The display in this and other 3-D figures is composed of three sections from the cube indicated by vertical and horizontal lines.

The full 2-D dataset and the estimated prestack slopes are shown in Figures 7 and 8, respectively. The output of migration to zero offset and stack is shown in Figures 9 (before stack) and 10 (after stack). All major events are properly transformed to the appropriate zero-offset positions.

Oriented prestack time migration

Mapping prestack data to the reflector position expressed in vertical traveltime is the task of prestack time migration. Analogously to dip moveout, prestack migration

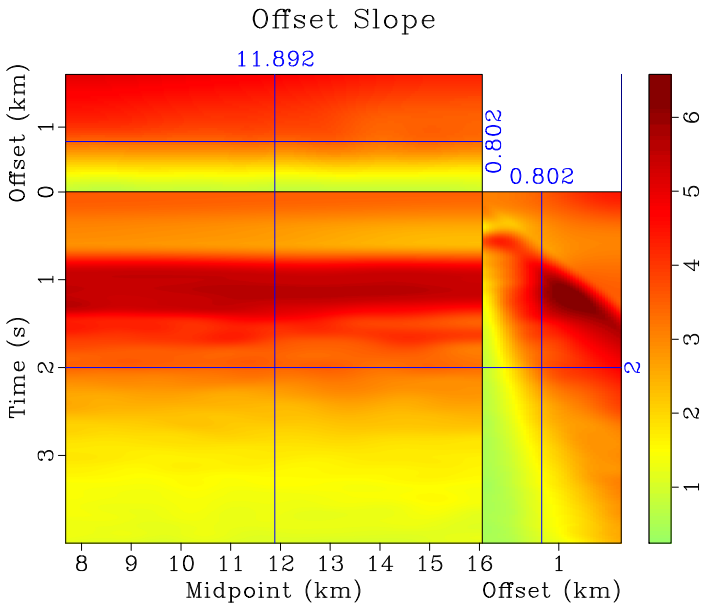

a

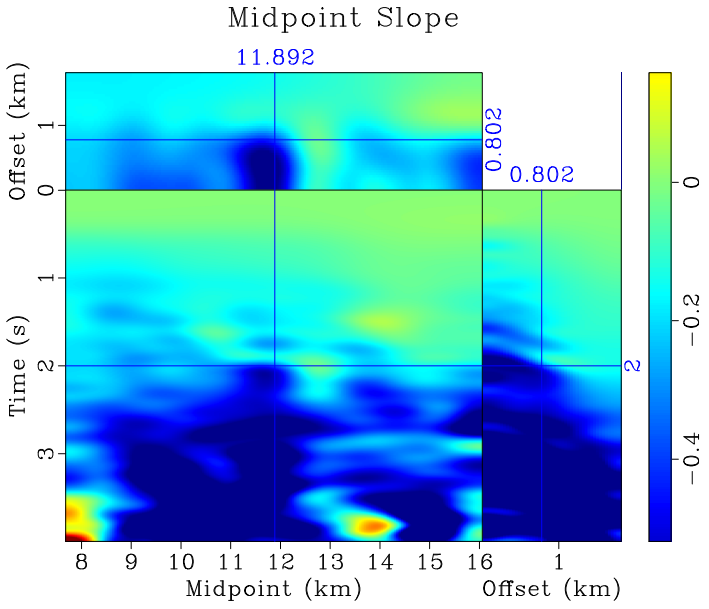

b

Figure 8: Prestack data slopes estimated from the dataset. a: Offset slope p_h. b: Midpoint slope p_y.

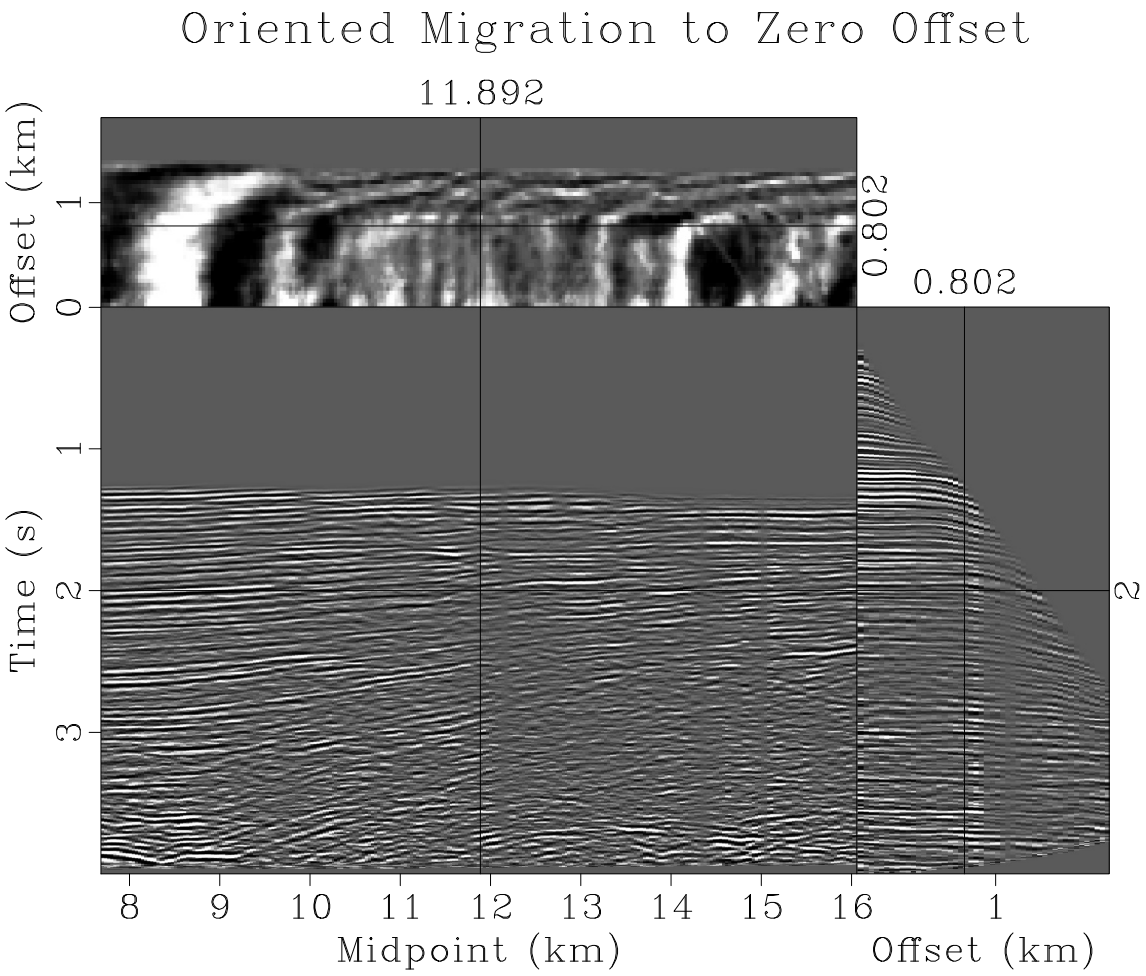

Figure 9: Output of oriented migration to zero offset.

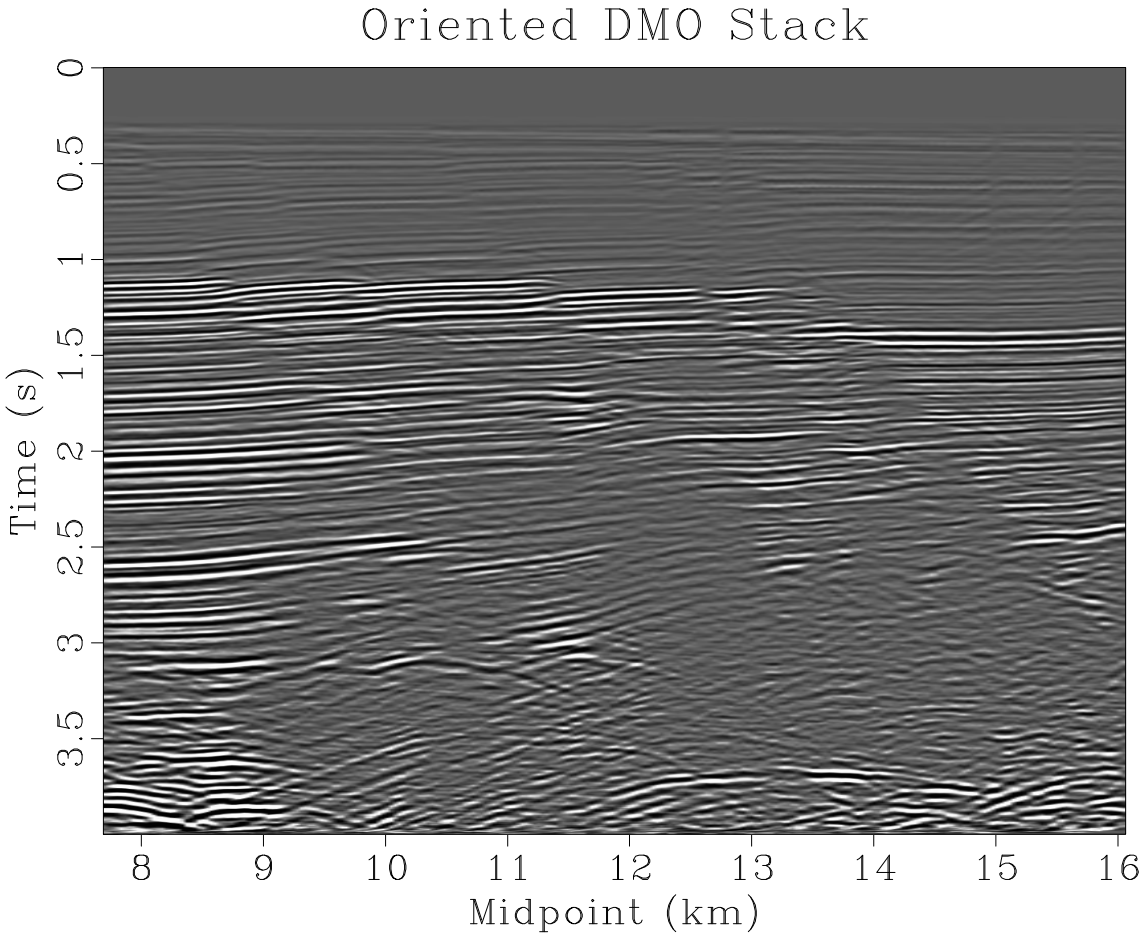

Figure 10: Seismic stack obtained by oriented migration to zero offset.

moves events not only across offsets but also across different midpoints provided that the reflectors are not flat. Using the oriented approach, mapping from the prestack domain $\{t, h, y\}$ to the time-migrated image domain $\{\tau, x\}$ is defined by the following equations derived in Appendix B:

$$\tau^2 = \frac{t\, p_h \left[(t - h\, p_h)^2 - h^2\, p_y^2\right]^2}{(t - h\, p_h)^2 \left[t\, p_h + h\, (p_y^2 - p_h^2)\right]}\,, \tag{18}$$

$$x = y - \frac{h\, t\, p_y}{t\, p_h + h\, (p_y^2 - p_h^2)}\,. \tag{19}$$

Here $\{\tau, x\}$ are the time-migrated image coordinates that correspond to the vertical ray traveltime and location (Hubral, 1977).

Under the assumption of a hyperbolic diffraction moveout, the migration velocity becomes, analogously to equation 4, a data attribute completely defined by prestack slopes, as follows:

$$\frac{4}{v^2} = \frac{t \left[t\, p_h + h\, (p_y^2 - p_h^2)\right]}{h\, (t - h\, p_h)}\,. \tag{20}$$

Equations 18 and 20 transform to equations 3 and 4 when $p_y = 0$, which corresponds to horizontal reflectors. Equations analogous to 18, 19, and 20 were derived previously by Billette et al. (2003) in a different way and in the depth imaging context.

Figures 11 and 12 show the output of prestack migration before and after stack. The result is comparable to that of conventional processing (Claerbout, 2005) but obtained two orders of magnitude faster, since each data point transforms directly to the image space through a one-to-one mapping instead of being spread along a wide migration impulse response, as in conventional prestack time migration.

DISCUSSION

The main advantage of the oriented approach is speed. The cost of velocity scanning in conventional processing (excluding the manual picking labor involved) can be estimated roughly as the number of scanned velocities N_v times the input data size. The cost increases dramatically in the case of non-hyperbolic approximations when more than one parameter needs to be picked. The cost of local slope estimation with the plane-wave destruction method is roughly the data size times the number of iterations N_i times the filter size N_f. Typically, $N_i \approx 10$ and $N_f = 6$, which is approximately equivalent in cost to scanning $N_v = 60$ velocities. The next step, however, is dramatically different. Since each data point is mapped directly to the image instead of being spread into a wide impulse response, we save the factor in cost proportional to the size (in samples) of the migration impulse response. The prestack migration result shown in Figure 11 was accomplished in under 10 seconds on a single-node PC.

The cost savings will be reduced somewhat if we take into account more than one local slope (crossing reflection events, diffractions, multiple reflections, etc.) The

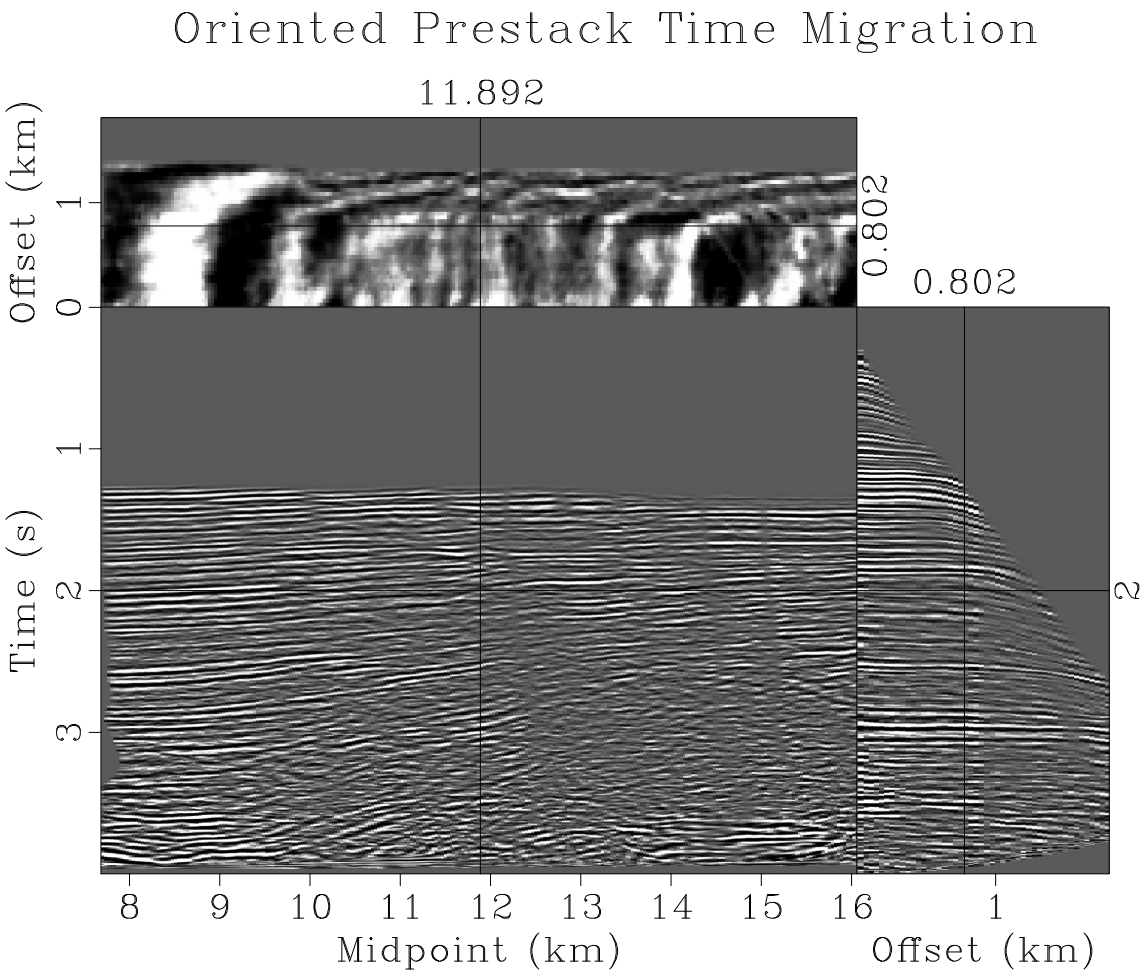

Figure 11: Output of oriented prestack time migration.

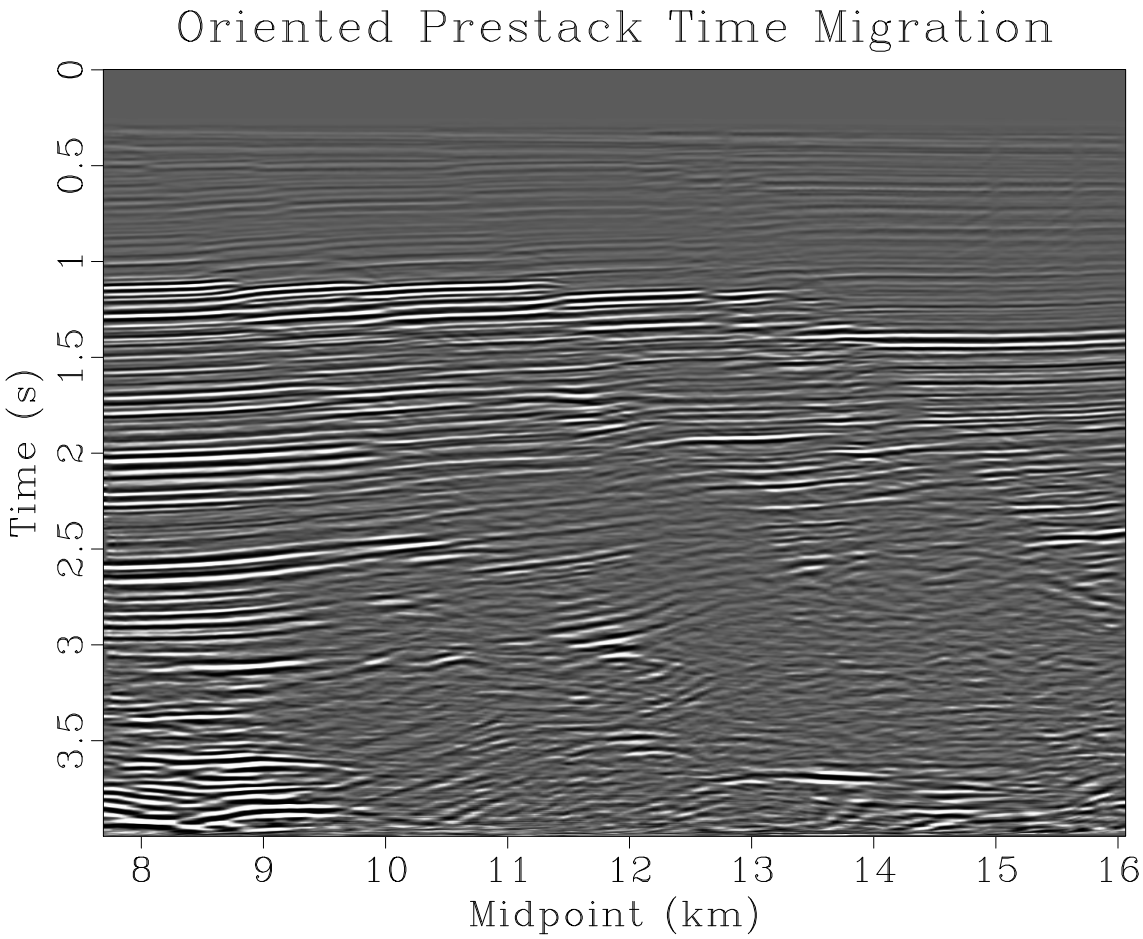

Figure 12: Seismic image obtained by oriented prestack time migration.

plane-wave destruction algorithm (Fomel, 2002) can be applied for estimating several interfering data slopes simultaneously. In order to take full advantage of it, data decomposition into local slope components may be required. The curvelet transform (Herrmann, 2003; Douma and de Hoop, 2006) suggests a possible data decomposition approach. To extend the method of curvelet imaging developed by Douma (2006), each local slope component would need to be imaged separately by an oriented approach with its contribution stacked into the final image.

Seismic imaging and velocity estimation is inherently an uncertain process because of limitations in the data acquisition geometry and signal bandwidth. In the oriented approach, the uncertainty in the velocity estimation and in the positioning of seismic reflectors comes directly from the uncertainty in estimating local event slopes. Such uncertainty is much easier to estimate and analyze in the oriented rather than in the traditional approach thanks to the explicit time-domain imaging equations 18 and 19 that transform uncertainties in the local event slopes p_h and p_y directly into uncertainties of the image point positioning.

CONCLUSIONS

Local slopes of seismic events contain complete information about the reflection geometry. Once they are estimated, one can turn seismic velocities and all other moveout parameters into data attributes directly mappable from the prestack data domain into the time-migrated image domain. In this paper, I have developed the analytical theory for this transformation and demonstrated its applicability with examples.

Extensions of oriented imaging from time to depth migration are provided in parsimonious migration (Hua and McMechan, 2003) using a ray tracing formalism and in the theory of the oriented wave equation (Fomel, 2003a) using a wave equation formalism.

ACKNOWLEDGMENTS

I would like to thank Jon Claerbout and Antoine Guitton for inspiring discussions. Huub Douma, Gilles Lambaré, Isabelle Lecomte, and one anonymous reviewer provided thorough and helpful reviews.

This publication is authorized by the Director, Bureau of Economic Geology, The University of Texas at Austin.

APPENDIX A

MATHEMATICAL DERIVATION OF ORIENTED DIX INVERSION

The famous Dix inversion formula (Dix, 1955) can be written in the form

$$v_i^2 = \frac{d}{d\,t_0}\left[t_0\,v^2(t_0)\right]\ , \tag{A-1}$$

where v_i is the interval velocity corresponding to the zero-offset traveltime t_0 and $v(t_0)$ is the vertically-variable root-mean-square velocity. By a straightforward application of the chain rule, I rewrite the Dix equation in the form

$$v_i^2 = \frac{d\,\left[t_0(t)\,v^2(t)\right]/d\,t}{d\,t_0/d\,t}. \tag{A-2}$$

Substituting $t_0(t)$ and $v(t)$ dependences from equations 3 and 4 and doing algebraic simplifications yields

$$\frac{d\,\left[t_0(t)\,v^2(t)\right]}{d\,t} = \frac{l}{p^2\,t}\,\frac{p\,l(p+t\,p_t)-2p_t\,t^2}{2\,t_0}\ , \tag{A-3}$$

$$\frac{d\,t_0}{d\,t} = \frac{2\,t-l\,(p+t\,p_t)}{2\,t_0}\ , \tag{A-4}$$

where $p_t = \partial p/\partial t$. Substituting equations A-3 and A-4 into A-2 produces equation 15 in the main text.

APPENDIX B

MATHEMATICAL DERIVATION OF ORIENTED TIME-DOMAIN IMAGING OPERATORS

The mathematical derivation of oriented time-domain imaging operators follows geometrical principles. Consider the reflection ray geometry in Figure B-1. Making a hyperbolic approximation of diffraction traveltimes used in seismic time migration is equivalent to assuming an effective constant-velocity medium and straight-ray geometry. The geometrical connection between the effective dip angle α, the effective reflection angle θ, the effective velocity v, half-offset h, and the reflection traveltime t is given by the equation

$$t = \frac{2\,h}{v}\,\frac{\cos\alpha}{\sin\theta}\ , \tag{B-1}$$

which follows directly from the trigonometry of the reflection triangle (Clayton, 1978; Fomel, 2003b). Additionally, the two angles are connected with the traveltime derivatives $p_h = \partial t/\partial h$ and $p_y = \partial t/\partial y$ according to equations

$$p_h = \frac{2\,\cos\alpha\,\sin\theta}{v}\ , \tag{B-2}$$

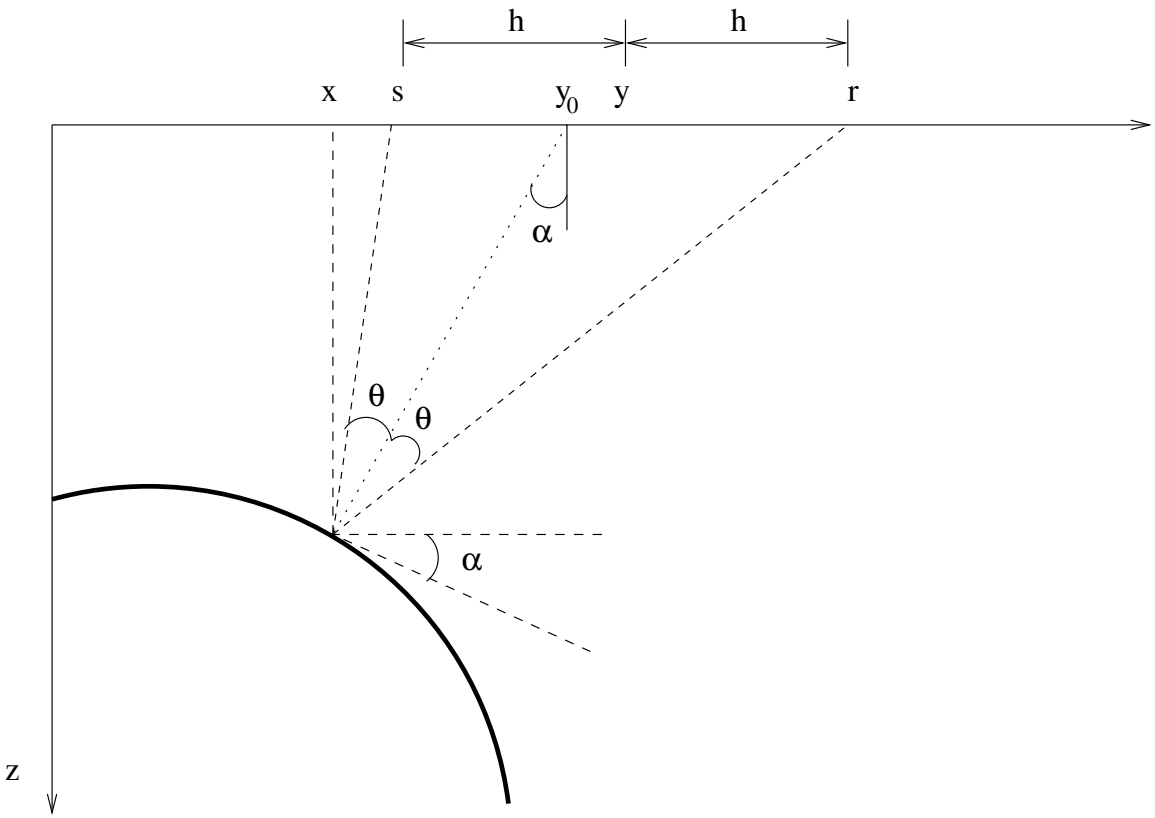

Figure B-1: Reflection ray geometry in an effectively homogeneous medium (a scheme).

$$p_y = \frac{2 \sin\alpha \cos\theta}{v} . \tag{B-3}$$

Using equations B-1, B-2, and B-3, one can explicitly solve for the effective parameters α, θ, and v expressing them in terms of the data coordinates t and h and event slopes p_h and p_y. The solution takes the form

$$\tan^2\alpha = \frac{h\, p_y^2}{p_h\,(t - h\, p_h)} , \tag{B-4}$$

$$\sin^2\theta = \frac{h\, p_h}{t} , \tag{B-5}$$

$$v^2 = \frac{4\, h\,(t - h\, p_h)}{t\,\left[t\, p_h + h\,(p_y^2 - p_h^2)\right]} . \tag{B-6}$$

Note that equation B-6 is equivalent to equation 20 in the main text. It reduces to equation 4 in the case of a horizontal reflector ($p_y = 0$).

With the help of equations B-4, B-5, and B-6, one can transform all other geometrical quantities associated with time-domain imaging into data attributes. The vertical two-way time is (Sava and Fomel, 2003)

$$\tau = t\,\frac{\cos^2\alpha - \sin^2\theta}{\cos\alpha\,\cos\theta} , \tag{B-7}$$

which turns, after substituting equations B-4 and B-5, into equation 18 in the main text. The separation between the midpoint and the vertical is (Sava and Fomel, 2003)

$$y - x = h\,\frac{\sin\alpha\,\cos\alpha}{\sin\theta\,\cos\theta} , \tag{B-8}$$

which turns, after substituting equations B-4 and B-5, into equation 19 in the main text. Additionally, the zero-offset traveltime is (using equation B-7)

$$t_0 = \frac{\tau}{\cos\alpha} = t\,\frac{\cos^2\alpha - \sin^2\theta}{\cos^2\alpha\,\cos\theta} , \tag{B-9}$$

which turns into equation 16. Finally, the separation between the midpoint and the zero-offset point is (using equations B-1 and B-8)

$$y - y_0 = y - x - \frac{v\,\tau}{2}\,\tan\alpha = h\,\tan\alpha\,\tan\theta , \tag{B-10}$$

which turns into equation 17. In the case of a horizontal reflector ($\alpha = 0$), $y = y_0 = x$, $t_0 = \tau$, and the zero-offset traveltime reduces to the NMO-corrected traveltime in equation 3.

Non-hyperbolic and three-dimensional generalizations of this theory are possible.

REFERENCES

Adler, F., and S. Brandwood, 1999, Robust estimation of dense 3-D stacking velocities from automated picking: 69th Ann. Internat. Mtg, Soc. of Expl. Geophys., 1162–1165.

Baina, R., S. Nguyen, M. Noble, and G. Lambare, 2003, Optimal antialiasing for ray-based depth Kirchhoff migration: 73rd Ann. Internat. Mtg., Soc. of Expl. Geophys., 1130–1133.

Billette, F., S. L. Begat, P. Podvin, and G. Lambare, 2003, Practical aspects and applications of 2D sterotomography: Geophysics, **68**, 1008–1021.

Billette, F., and G. Lambaré, 1998, Velocity macromodel estimation from seismic reflection data by stereotomography: Geoph. J. Internat., **135**, 671–680.

Castle, R. J., 1994, Theory of normal moveout: Geophysics, **59**, 983–999.

Claerbout, J. F., 1992, Earth Soundings Analysis: Processing Versus Inversion: Blackwell Scientific Publications.

———, 2005, Basic Earth imaging: Stanford Exploration Project, `http://sepwww.stanford.edu/sep/prof/`.

Clayton, R. W., 1978, Common midpoint migration, *in* SEP-14: Stanford Exploration Project, 21–36.

de Bazelaire, E., 1988, Normal moveout revisited - Inhomogeneous media and curved interfaces: Geophysics, **53**, 143–157.

Dix, C. H., 1955, Seismic velocities from surface measurements: Geophysics, **20**, 68–86.

Douma, H., 2006, A hybrid formulation of map migration and wave-equation-based migration using curvelets: PhD thesis, Colorado School of Mines.

Douma, H., and M. de Hoop, 2006, Leading-order seismic imaging using curvelets, *in* 76th Ann. Internat. Mtg.: Soc. of Expl. Geophys, accepted.

Fomel, S., 2002, Applications of plane-wave destruction filters: Geophysics, **67**, 1946–1960.

———, 2003a, Angle-domain seismic imaging and the oriented wave equation: 73rd Ann. Internat. Mtg., Soc. of Expl. Geophys., 893–898.

———, 2003b, Velocity continuation and the anatomy of residual prestack time migration: Geophysics, **68**, 1650–1661.

———, 2007, Shaping regularization in geophysical estimation problems: Geophysics, accepted for publication.

Fomel, S., and V. Grechka, 2001, Nonhyperbolic reflection moveout of P waves. An overview and comparison of reasons, *in* CWP-372: Colorado School of Mines.

Hale, D., 1995, DMO processing: Soc. of Expl. Geophys.

Herrmann, F., 2003, Optimal seismic imaging with curvelets: 73rd Ann. Internat. Mtg., Soc. of Expl. Geophys., 997–1000.

Hertweck, T., C. Jäger, J. Mann, E. Duveneck, and Z. Heilmann, 2004, A seismic reflection imaging workflow based on the Common-Reflection-Surface (CRS) stack: theoretical background and case study, *in* 74th Ann. Internat. Mtg: Soc. of Expl. Geophys., 2032–2035.

Hua, B., and G. A. McMechan, 2003, Parsimonious 2D prestack Kirchhoff dept mi-

gration: Geophysics, **68**, 1043–1051.

Hubral, P., 1977, Time migration - Some ray theoretical aspects: Geophys. Prosp., **25**, 738–745.

Lambaré, G., 2004, Stereotomography: Where we are, and where we should go: 74th Ann. Internat. Mtg., Soc. of Expl. Geophys., 2367–2370.

Lambaré, G., M. Alerini, R. Baina, and P. Podvin, 2004a, Stereotomography: a semi-automatic approach for velocity macromodel estimation: Geophysical Prospecting, **52**, 671–681.

Lambaré, G., M. Alerini, and P. Podvin, 2004b, Stereotomographic picking in practice, *in* 74th Ann. Internat. Mtg: Soc. of Expl. Geophys., 2343–2346.

Landa, E., B. Gurevich, S. Keydar, and P. Trachtman, 1999, Application of multifocusing for subsurface imaging: Applied Geophysics, **42**, 283–300.

Malovichko, A. A., 1978, A new representation of the traveltime curve of reflected waves in horizontally layered media: Applied Geophysics (in Russian), the translation provided by Sword (1987a), **91**, 47–53.

Ottolini, R., 1983, Velocity independent seismic imaging, *in* SEP-37: Stanford Exploration Project, 59–68.

Riabinkin, L. A., 1957, Fundamentals of resolving power of controlled directional reception (CDR) of seismic waves, *in* Slant-stack processing, 1991: Soc. of Expl. Geophys. (Translated and paraphrased from *Prikladnaya Geofiizika*, **16**, 3-36), 36–60.

Rieber, F., 1936, A new reflection system with controlled directional sensitivity: Geophysics, **01**, 97–106.

Sava, P. C., and S. Fomel, 2003, Angle-domain common-image gathers by wavefield continuation methods: Geophysics, **68**, 1065–1074.

Siliqi, R., and N. Bousquié, 2000, Anelliptic time processing based on a shifted hyperbola approach: 70th Ann. Internat. Mtg, Soc. of Expl. Geophys., 2245–2248.

Siliqi, R., D. L. Meur, F. Gamar, L. Smith, J. Toure, and P. Herrmann, 2003, High-density moveout parameter fields V and Eta, Part 1: Simultaneous automatic picking: 73rd Ann. Internat. Mtg., Soc. of Expl. Geophys., 2088–2091.

Stoffa, P. L., P. Buhl, J. B. Diebold, and F. Wenzel, 1981, Direct mapping of seismic data to the domain of intercept time and ray parameter - A plane-wave decomposition: Geophysics, **46**, 255–267.

Sword, C. H., 1987a, A Soviet look at datum shift, *in* SEP-51: Stanford Exploration Project, 313–316.

———, 1987b, Tomographic determination of interval velocities from reflection seismic data: The method of controlled directional reception: PhD thesis, Stanford University.

Wolf, K., D. Rosales, A. Guitton, and J. Claerbout, 2004, Robust moveout without velocity picking, *in* 74th Ann. Internat. Mtg: Soc. of Expl. Geophys., 2423–2426.

Yilmaz, O., 2000, Seismic data analysis: Soc. of Expl. Geophys.